

## Article

# Model of the Temperature Influence on Additively Manufactured Carbon Fibre Reinforced Polymer Samples with Embedded Fibre Bragg Grating Sensors

Torkan Shafighfard  and Magdalena Mieloszyk \* 

Institute of Fluid Flow Machinery, Polish Academy of Sciences, Fiszerka 14, 80-231 Gdansk, Poland; tshafighfard@imp.gda.pl

\* Correspondence: mmieloszyk@imp.gda.pl

**Abstract:** This study investigates the thermo-mechanical behaviour of additively manufactured Carbon Fiber Reinforced Polymer (CFRP) with embedded Fibre Bragg Grating (FBG) sensors with respect to their feasibility for utilising them under thermal loading. This was conducted through the Finite Element Method (FEM) inside an ABAQUS environment. Numerical simulation was complemented by several experimental investigations in order to verify the computational results achieved for the specimens exposed to thermal loading. FBG sensors, incorporated into the material by embedding technique, were employed to measure the strains of the samples subjected to elevated temperatures. It was shown that the strains given by numerical simulation were in good agreement with the experimental investigation except for a few errors due to the defects created within the layers during Additive Manufacturing (AM) process. It was concluded that the embedding FBG sensors were capable of identifying thermo-mechanical strain accurately for 3D-printed composite structures. Therefore, the findings of this article could be further developed for other types of material and loading conditions.



**Citation:** Shafighfard, T.; Mieloszyk, M. Model of the Temperature Influence on Additively Manufactured Carbon Fibre Reinforced Polymer Samples with Embedded Fibre Bragg Grating Sensors. *Materials* **2022**, *15*, 222. <https://doi.org/10.3390/ma15010222>

Academic Editor: Agnieszka Jastrzębska

Received: 10 November 2021  
Accepted: 24 December 2021  
Published: 28 December 2021

**Publisher's Note:** MDPI stays neutral with regard to jurisdictional claims in published maps and institutional affiliations.



**Copyright:** © 2021 by the authors. Licensee MDPI, Basel, Switzerland. This article is an open access article distributed under the terms and conditions of the Creative Commons Attribution (CC BY) license (<https://creativecommons.org/licenses/by/4.0/>).

**Keywords:** Additive Manufacturing; composite; temperature; fused deposition modelling; Finite Element Method; Fibre Bragg Grating

## 1. Introduction

Additive Manufacturing (AM), so-called 3D printing, is a layer by-layer fabrication process in which successive layers of the material are deposited above each other taking advantage of a computer aided design to form the final product [1]. Thanks to the recent development in technology and the current trend toward a sustainable environment [2], it has been widely utilised in various industrial applications such as aeronautical, automotive, dental, architectural, and medical sectors for fabrication of various prototypes, particularly with complex geometries since it provides superior design flexibility compared to conventional manufacturing methods [3]. Therefore, it is believed that the AM will be the third industrial revolution, complementing the production line assembly that dominated manufacturing starting in the previous century [4].

Technology development was not limited to the manufacturing processes. Correlating with the fabrication techniques, the desire toward making the materials more efficient, e.g., smart materials have been among the significant goals of science and industry. Therefore, demand for composite materials has notably been increased during the past decade due to their high stiffness-weight ratio [5], as well as corrosion resistance, decorativeness, and thermal stability. On the other hand, the intrinsic sensing capabilities they own make them suitable for Structural Health Monitoring (SHM) in aerospace and mechanical engineering applications [6].

Meanwhile, since composite materials are subjected to different mechanical and/or thermal loading, which decreases the structural performance, it has been essential to develop a reliable and precise real-time monitoring method in order to obtain information

on the structural state of material to improve the performance of composite products [7–9]. Surface mounted optical fibre sensors have obtained remarkable attention in the field of experimental stress analysis and health monitoring of composite structures [10]. Fibre Bragg grating (FBG) sensor has been preferred while embedding into composite structures to other types of sensors due to their small dimension and low weight, corrosion resistance as well as multiplexing capability and high sensitivity [11]. It is worth highlighting that the effect of FBG sensors embedding on structural durability is very limited. A FBG sensor is a type of distributed Bragg reflector constructed in a short segment of optical fiber that reflects particular wavelengths of light and transmits all others. The operation of FBG is based on the measurement of the changes in a reflective signal, which is the center wavelength of back-reflected light from a Bragg grating, depending on the effective refractive index of the core and the periodicity of the grating [12]. The deficiency of trusted reliable in-situ monitoring for purposes of controlling the building process and final product quality has prevented AM technology from developing [13], thereby embedding FBG sensors within composite structures is necessary for real-time monitoring of temperature alterations and measurements of induced residual strains. It is also a highly innovative and promising technique in order to identify significant process defects while manufacturing samples [14]. Temperature [15] and strain [16] have been mostly measured in Structural Health Monitoring systems through FBG sensors.

Conventional methods could be utilised in order to embed FBG sensors into composite specimens during manufacturing process [17,18]. Additively manufactured pure polymeric specimens could also contain FBG sensors employing e.g., multi-jet printing [19,20] or Fused Deposition Modelling (FDM) [21,22] techniques. It was shown that the structural performance of the pure polymers could be improved significantly via integrating them with short fibre [23–25] and/or continuous fibre [26–28], while 3D printing with the FDM method.

Notwithstanding the advantages of the FDM process to fabricate composite structures, it is not totally perfect. The quality and strength of the printed sample are negatively affected by the possible defects corresponding to the FDM method [29,30]. Among these defects, thermal gradients are the most important one that causes the flaws in the specimen during the manufacturing process since it encounters sequential melting and rapid cooling cycles of the deposited material. It can lead to detrimental residual stresses, resulting in delamination failure [31,32]. Hence, the temperature history of the manufactured product via the FDM technique should be studied. Temperature variation has a significant role on assessing the quality of bond formation on the interface of neighbour filaments and mechanical properties of the structure [33]. An experimental study was conducted to measure the internal strains while manufacturing the polymeric structures with FBG sensors [34]. The magnitude of the induced residual strains in FDM built composite structures were measured using FBG sensors and the effect of layer thickness was investigated [35]. The behaviour of the coefficient of thermal expansion for carbon and the glass fiber reinforced polymer specimens as well as the effect of the stacking sequence on the residual strain and temperature profiles were studied [36]. AM technique was utilised for different materials including Carbon Fiber Reinforced Polymers (CFRP) and Poly(lactic acid) (PLA) to insert FBG sensors at the subsurface of the material or in-depth in various locations with a condition of sensors integrity and reliability of measured values [37]. The internal temperature change of different PLA and CFRP specimens were investigated during the AM process through FBG sensors [38]. FBG sensors were utilised to characterise the deformations and residual strains in additively manufactured plates by FDM [39]. Recently, the thermal strain of the FDM-fabricated composite sample due to its exposition on elevated temperature was studied employing FBG sensors. The numerical analyses were conducted to understand the influence of the elevated temperature on AM composite structure with continuous carbon fibre reinforcement. The analyses considered the influence of the fibre reinforcement occurrence and the thickness of the fibre bundles on matrix thermal stability [40]. On the other hand, the main focus of the current paper is on FBG sensors and their influence on the structure as well as their utility for the strain measurement during temperature elevation.

The temperature effect on the mechanical behaviour of the 3D printed CFRP specimens was also studied. 3D printed materials with carbon fibre reinforcement were modeled using the Finite Element Analysis software package. Moreover, this paper expanded the investigation in numerical methods in order to analyse the thermomechanical behaviour of the sample model which was exposed to global thermal loading same as which was carried out in the experimental condition. The simulation results were finally validated using experimental work performed at an environmental chamber using FBG sensors embedded into the CFRP material structure.

Mechanical characterisation of CFRP samples has been studied during the FDM process and has not undergone the 3D printed components itself, in several research articles. Also, a few investigations were carried out for the temperature elevation effect on the mechanical behaviour of composite structures specifically to the heat deflection temperature of PLA. Therefore, in this article, CFRP specimens were additively manufactured through FDM process and tested on an environmental chamber to investigate the effect of the temperature elevation on the mechanical behaviour of those samples. The fabricated specimens were also modelled in the Finite Element Analysis software package, ABAQUS in order to simulate the thermo-mechanical behaviour of the manufactured specimens under thermal loading. The resulted simulation was validated using experimental work performed at an environmental chamber using FBG sensors embedded into the CFRP material structure.

## 2. Samples

### 2.1. Manufacturing Method

The chosen AM method for CFRP material was a modified FDM method developed by project partner (Kaunas University of Technology, Kaunas, Lithuania), who designed their own solution of the printing head [41]. MeCreator 2 3D printer of Geeetech with the printing parameters represented in Table 1, Ref. [41] was utilised in order to fabricate the samples.

**Table 1.** Parameters used for fabricating the sample [41].

First Layer [mm/s]	Speed		Temperature		Extrusion	
	Printing [mm/s]	Fan [%]	Extruder [°C]	Bed [°C]	Multiplier [mm]	Width [mm]
1.20	4	50/80/100	200	70	0.6	1.6

### 2.2. Sample

The analysed structures are three CFRP specimens with the same dimensions and manufactured using the same AM technique. Their dimensions are listed in Table 2. For the matrix, PLA with DR3D Filament of the diameter 1.75 mm was utilised, while as the reinforcement, the carbon fiber T300B-1000 with the diameter of 1.75  $\mu\text{m}$  from the Toray was chosen. A photograph of one sample and its scheme with marked FBG sensors locations are presented in Figure 1. In the middle of each sample (between the 2nd and the 3rd layer), the FBG sensor (denoted as  $S_w$ ) was embedded. Additionally, on each sample surface, another sensor (denoted as  $S_z$ ) was glued using cyanoacrylate glue. Both FBG sensors (10 mm gauge length) were aligned parallel with the carbon fiber direction.

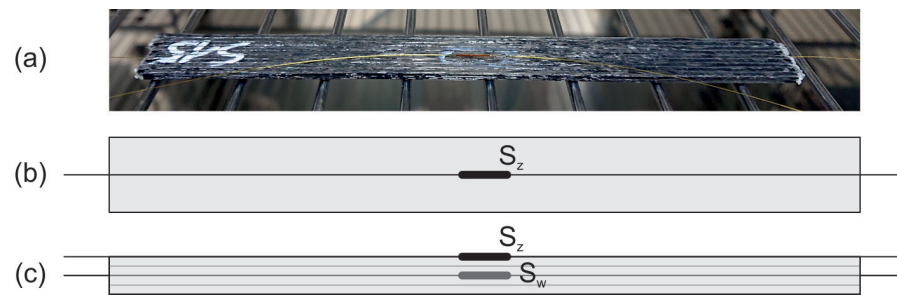


**Figure 1.** Sample: (a) Photograph and scheme, (b) top view of the sample, and (c) cross-section of the sample;  $S_z$ —FBG sensor glued on the surface,  $S_w$ —FBG sensor embedded.

**Table 2.** Specimen dimensions.

Length [mm]	Sample		Layer		Stacking Sequence
	Width [mm]	Thickness [mm]	Thickness [mm]	Number	
150	15	2	0.5	4	[0, 0] s

An example of comparison of FBG sensor spectra before and after embedding is presented in Figure 2. It is observed that the embedding process results in the reduction of sensor reflectivity (amplitude reduction) but does not influence the spectrum shape. Therefore, the embedded sensors can be applied for measurements.

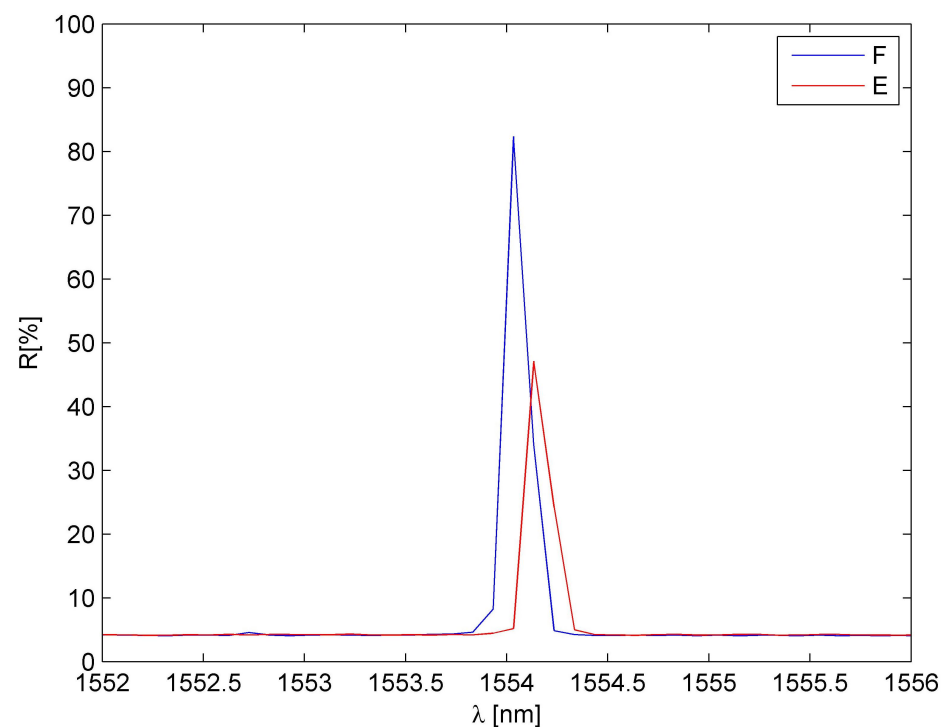


**Figure 2.** A comparison of FBG sensor spectra: F—free, E—after embedding.

The mechanical properties of the materials used for manufacturing the samples are collected in Table 3. The values were given by the manufacturers or achieved from experimental tests [41].  $E$ ,  $\rho$ ,  $\nu$ ,  $X_t$ ,  $\nu$ ,  $\kappa$ , and  $C$  are elastic modulus, density, Poisson ratio, failure strength, volume fraction, thermal conductivity, and heat capacity, respectively.

**Table 3.** Specimen parameters.

	E [GPa]	$\rho$ [g/cm <sup>3</sup> ]	$\nu$	$\chi_t$ [MPa]	$\nu$ [%]	$\kappa$ [W/mK]	C [J/kgK]
Fibre	230	176	0.33	3530	18	10.46	794
Matrix	2.315	1.24	0.29	51	82	0.13	1800

### 3. Experimental and Numerical Investigation

The influence of elevated temperatures on the CFRP samples was analysed experimentally and numerically. The samples were exposed to eight temperature values: 10 °C, 15 °C, 20 °C, 25 °C, 30 °C, 35 °C, 40 °C, and 45 °C. The maximal temperature was related to Tg temperature of the used PLA material. Generally, the Tg of PLA lies between 50 °C and 70 °C [42]. Based on the Dynamic Mechanical Analysis (DMA), performed on the PLA material, it has the relatively low deflection temperature value as of 42 °C [40].

The investigations were performed under stable Relative Humidity (RH) values, equal to 20%. For both numerical and experimental investigations, the base temperature was equal to 20 °C.

#### 3.1. Coefficient of Thermal Expansion of PLA

Firstly, the Coefficient of Thermal Expansion (CTE) of the PLA matrix was determined experimentally. It was performed on the sample manufactured under the same manufacturing conditions as the CFRP samples but without adding the fibre reinforcement. The sample dimensions were 50 mm (length)  $\times$  20 mm (width)  $\times$  10 mm (thickness). In the middle of the sample, an FBG sensor was embedded. The sample photograph and cross-section scheme with marked FBG sensor location is presented in Figure 3.

**Figure 3.** A photograph and cross-section scheme of the PLA sample.

The measurement was performed in environmental chamber MyDiscovery DM600C (Angelantoni Test Technologies Srl, Massa Martana, Italy). During the investigation, the sample was on the shelf, so it has the possibility to expand in all directions. The measurements were performed using interrogator si425-500 from Micron Optics with a measurement frequency equal to 1 Hz.

Total strain  $\varepsilon_c$  values for the FBG sensor was calculated using the following equation:

$$\varepsilon_c(T) = \frac{\lambda_p(T) - \lambda_b(T)}{\lambda_b(T)} \quad (1)$$

where  $\lambda_p$  and  $\lambda_b$  are measured and base Bragg wavelengths, respectively.

Strain values related to the temperature influence on the PLA material was determined using the following relationship:

$$\varepsilon_m(T) = \varepsilon_c(T) - \varepsilon_f(T) \quad (2)$$

where index  $m$  is related to the material, while index  $f$  is linked with the influence of the temperature on the FBG sensor material. Then, for the purpose of determining the relationship between strain and temperature for the PLA material the following equation was applied:

$$\varepsilon_T = \frac{1}{n} \sum_{i=1}^n \varepsilon_n(T_i) \text{ for } i = 1, \dots, 8; n = n_1, \dots, n_n; \quad (3)$$

where temperature level  $T_i$  is related to averaged temperature value from  $n$  points for stable temperature conditions lasting 300 s. The calculation error for temperature was  $0.36 \text{ }^\circ\text{C}$ , whereas that for the strain was  $3.6 \times 10^{-6} \text{ m/m}$ .

Strain values determined for the PLA material are presented in Figure 4. It is well visible that up to  $40 \text{ }^\circ\text{C}$ , the relationship between strain and temperature is linear. It can be described using the relationship:

$$\varepsilon_{PLA}^a(T) = P_1T + P_2. \quad (4)$$

The linear approximation is denoted as a black line in Figure 4. The measurement point for  $45 \text{ }^\circ\text{C}$  is not laying on the same straight line, so a correction was introduced. The observed material behaviour is probably related to the deflection temperature of the PLA material. The detailed discussion related to the temperature influence on the PLA material is presented in [40]. So, the relationship between strain and temperature for temperatures higher than  $40 \text{ }^\circ\text{C}$  was approximated using linear relationship but with different polynomial constants. The approximation was denoted as a red line in Figure 4. Both polynomial constants are collected in Table 4.

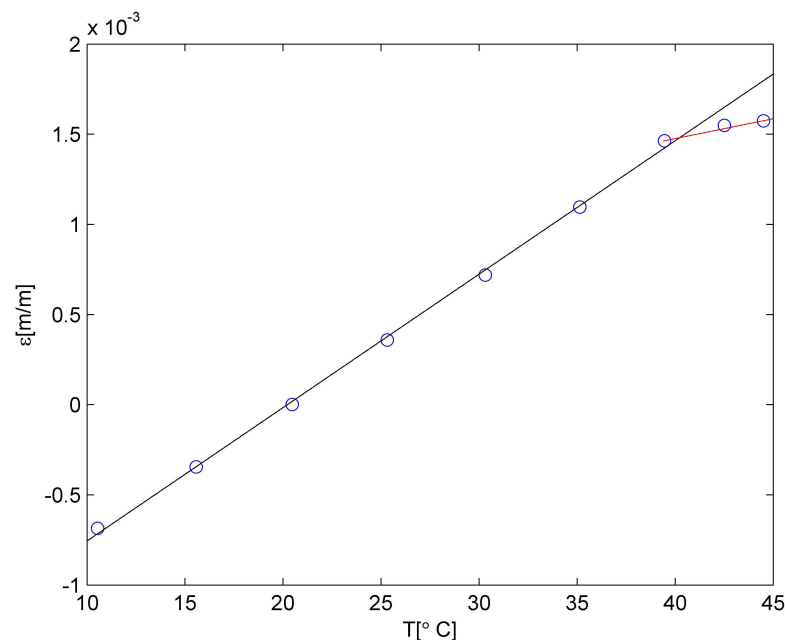


Figure 4. Strain in PLA material due to the temperature influence.

**Table 4.** Polynomials constants.

	First Approximation ( $\times 10^{-5}$ )	Second Approximation ( $\times 10^{-5}$ )
$P_1$	7.40	−149.55
$P_2$	2.20	59.58
line in Figure 4	black	red

The thermal expansion coefficient is the first derivative of Equation (4) calculated using the relationship:

$$\alpha(T) = \frac{\partial \varepsilon(T)}{\partial T}. \quad (5)$$

Therefore, the CTE for the PLA matrix is equal to  $7.40 \times 10^{-5} \text{ m/m } ^\circ\text{C}$  for temperatures lower than  $40 \text{ } ^\circ\text{C}$  and  $2.20 \times 10^{-5} \text{ m/m } ^\circ\text{C}$  for temperatures higher than  $40 \text{ } ^\circ\text{C}$ . Such values were used for numerical calculations.

The observed material behaviour was similar to the one determined by FBG sensor embedded into ABS using the FDM method [22]. There are observed differences between the PLA material behaviour and the previously exterminated M3 crystal, also manufactured using a 3D printer [1]. The relationship between strain and temperature for M3 crystal was described by a second degree polynomial instead of a linear function (also for the temperatures significantly lower than the glass transition temperature). The observed differences between the materials can be not only related to the material properties but also the used manufacturing technique. The M3 crystal samples were manufactured using multi-jet printing (MJP) method, while the PLA was made by FDM. The MJP offers very high accuracy of elements (the layer thickness is equal to  $16 \text{ } \mu\text{m}$ ), but cannot be implemented to manufacturing CFRP elements [1].

### 3.2. Numerical Calculation

The material behaviour corresponding to the effect of the temperature on the CFRP samples was modelled using the Finite Element Method (FEM). Abaqus [43] software was employed in this study for numerical analysis. The ply-by-ply technique was used to model the finite element of the composite laminate. Material orientations with mechanical properties given in Table 2 were assigned to each ply considering their orientation angle for the stated stacking sequence (total of 4 plies). In order to find an optimum number of elements inside the FEM model and avoid high consuming times and achieve an acceptable deviancy, the convergence study was carried out. Therefore, 9000 quadratic hexahedral fully-integrated elements (C3D20RT) with a total of 45,069 nodes were used in the FEM model. The convergence issue was removed while setting seeds size at a similar distance of 1 mm on every edge. It should be mentioned that the bottom part of the sample, which was put on a shelf in the chamber during measurements, was restricted to move in the thickness direction, while one side of the sample was restricted to move in the  $y$ -direction and another side restricted in the  $x$ -direction in order to let the sample expanded. The temperature elevation was input to the software as a time-amplitude loading. Finally, the pre-defined temperature of  $20 \text{ } ^\circ\text{C}$  was defined for the sample due to the initial temperature of the chamber. The boundary conditions and model were shown in Figure 5.

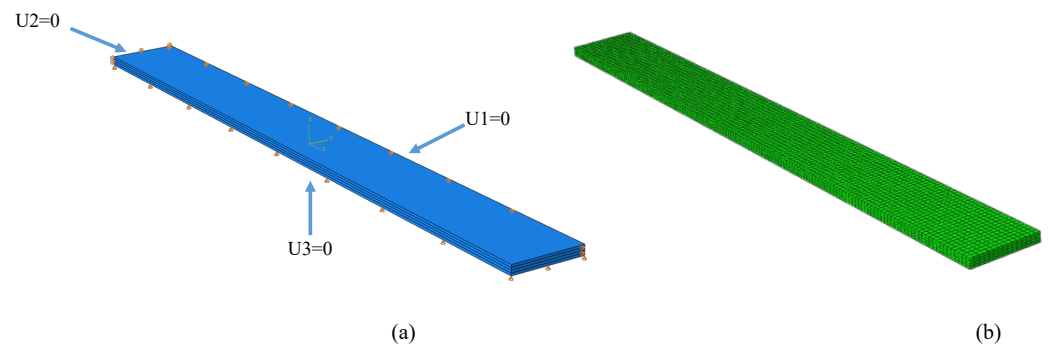


**Figure 5.** FEM model: (a) Boundary conditions and (b) meshed model.

It was assumed that the temperature corresponding to base conditions was equal to 20 °C. Temperature values were given to the FEM model as an amplitude.

In addition, the emissivity ( $\epsilon_s = 0.96$ ) was considered for the CFRP sample since it was exposed to thermal radiation that occurred inside an environmental chamber. It should be mentioned that this radiation was applied to all the surfaces since they were in interaction with the ambient. For thermal conductivity, the upper and lower bounds, parallel and serial, were used to estimate the composite properties. The thermal conductivity parameters along the longitudinal and transverse directions to the fiber were provided by:

$$\kappa_u = k_f v_f + k_m v_m \quad (6)$$

$$\kappa_t = \frac{k_f k_m}{k_m v_f + k_f v_m}. \quad (7)$$

In which the  $\kappa_f$ ,  $\kappa_m$ ,  $v_f$ , and  $v_m$  are thermal conductivity of the fiber, thermal conductivity of the matrix, fiber volume fraction, and matrix volume fraction, respectively.

In addition, the coefficient of thermal expansion for longitudinal and transverse direction to the fiber were found respectively by:

$$\alpha_{11} = \frac{v_f \alpha_f E_f + v_m \alpha_m E_m}{v_f E_f + v_m E_m} \quad (8)$$

$$\alpha_{22} = \alpha_f v_f + \alpha_m v_m. \quad (9)$$

Wherein,  $\alpha_f$ ,  $\alpha_m$ ,  $v_f$ , and  $v_m$  are the coefficient of thermal expansion and volume fraction of fiber and matrix, respectively.

### 3.3. Experimental Investigation

Then the experimental investigation of the influence of temperature on the CFRP samples was performed in the environmental chamber. During the investigation, the CFRP samples were kept on the shelf, similarly like the PLA sample. In addition, the same interrogator with the same measurement frequency was applied. The temperature values in the samples location were measured using the FBG temperature probe. The measurements were performed twice and the analyses were performed on the averaged values of the measured Bragg wavelengths.

The total strain values for all FBG sensors are presented in Figure 6. The values were calculated using Equation (1). The average strain variation determined for all sensors was equal to  $5 \times 10^{-6}$ , while the measurement accuracy of the interrogator was equal to  $2 \times 10^{-6}$ . It is well visible that all curves registered for strain sensors have the same shape as the temperature curve. All sensors embedded in the samples ( $S1_w$ ,  $S2_w$ ,  $S3_w$ ) have similar strain values, so it can be assumed that they present the averaged strain of the CFRP material. The averaged difference among the strain values determined for the same temperatures is equal to  $4 \times 10^{-6}$ . While for the sensors mounted on the samples surfaces,

differences can be observed. They are related to the FBG sensors location on the carbon fibre and the matrix ( $S1_z$  and  $S3_z$ ) or on the carbon fibre bundle ( $S2_z$ ). Due to observed differences among sensors, the results were not used for the consecutive calculations and the FEM model evaluation.

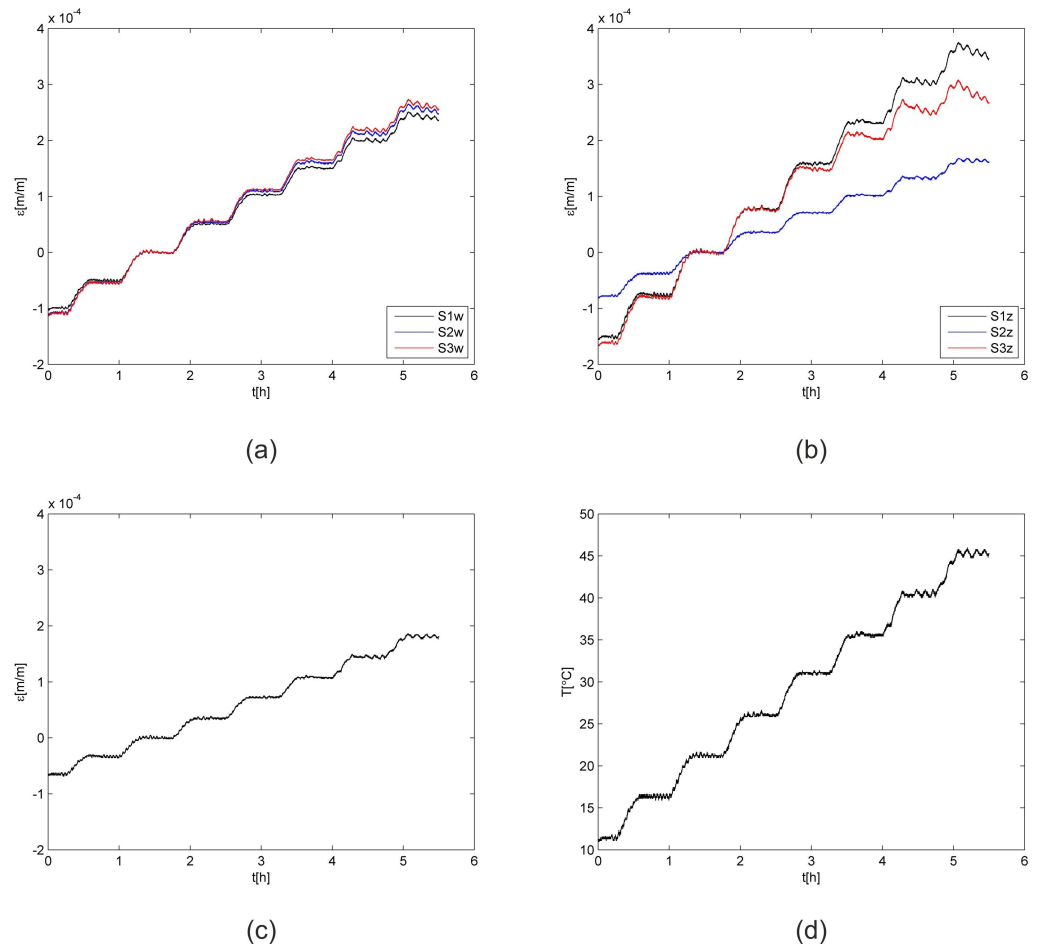


**Figure 6.** Total strain: (a) Embedded sensors, (b) sensors on the surfaces, (c) free sensor, and (d) temperature; S1,S2,S3—CFRP samples.

Then CFRP strain values were determined using the same procedure as was described for the PLA matrix. The relationship between the temperature and strain is presented in Figure 7.

It is well visible that the relationship is quadratic. For a CFRP 3D-printed sample utilised in this study, the error was calculated to be 2%. This error may be considered statistically negligible and excluded from statistical evaluation.

The average percentage deviation between the experimental and approximation was calculated using Equation (10):

$$\epsilon_e(T) = \frac{\epsilon_E - \epsilon_A}{\epsilon_E}. \quad (10)$$

In which  $E$  refers to an experimental and  $A$  refers to an approximated values of the normal strain, respectively.

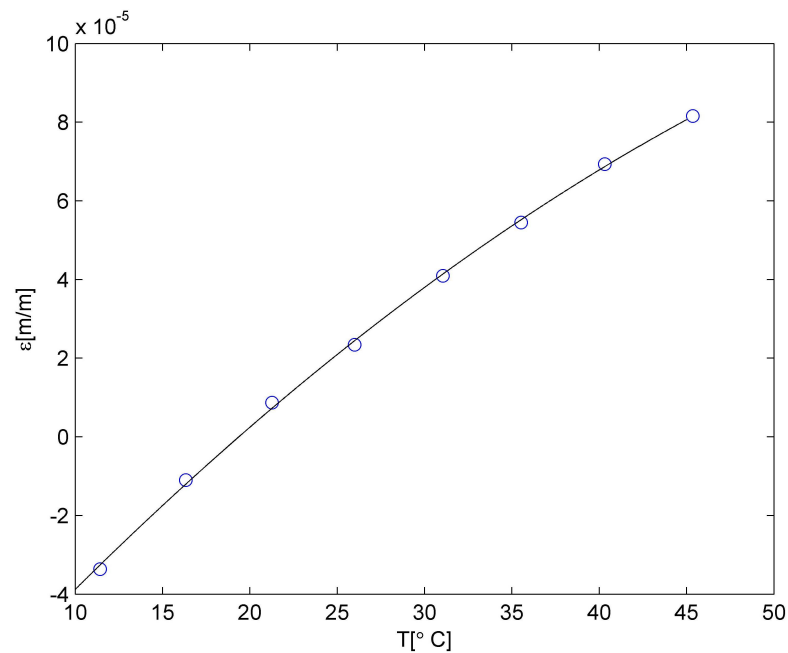


**Figure 7.** Relationship between strain and temperature for CFRP samples.

The obtained numerical results of the temperature and strain relationship were compared with the experimental data. The comparative plots are shown in Figure 8. The model values (marked by blue circles) were calculated using the first CTE value of the PLA material. For such an assumption, the average strain difference is equal to  $1.20 \times 10^{-6}$  for the whole range of temperatures. It is related to 7% differences. Taking into consideration the 45 °C only, the strain difference is equal to  $9.74 \times 10^{-6}$ . The model correction related to the PLA matrix material characteristic—CTE value of PLA material – allows for decreasing the difference to  $1.58 \times 10^{-6}$ . Due to the fact that the material behaviour change influenced the one temperature only, the averaged percentage difference was reduced to 5% only.

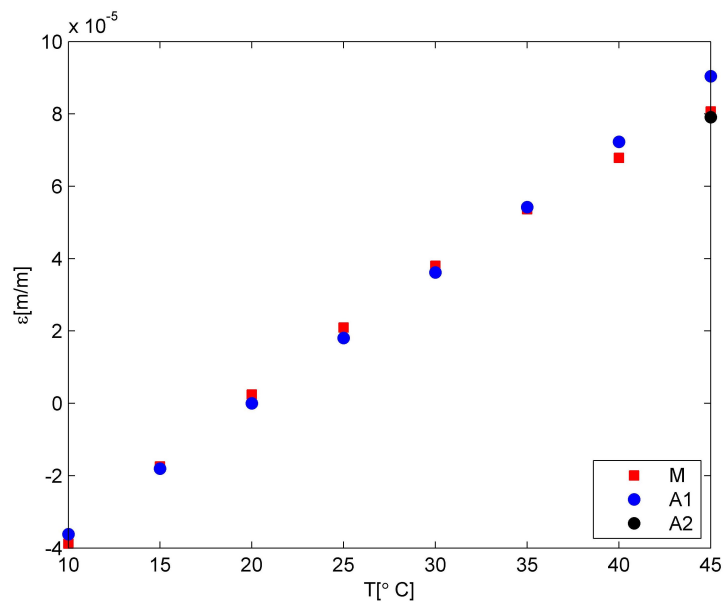


**Figure 8.** Comparison between model and experiment; M—measurement, A1—model with the first CTE value for PLA, A2—model with the CTE value correction for higher temperatures.

#### 4. Conclusions

A 4-layer composite unidirectional laminate was fabricated employing AM, FDM technique. The numerical results were compared to the averaged strain values for three samples for measurements repeated twice. The effect of the elevated temperature on the thermal strain of the 3D-printed specimens was studied. Both experimental and numerical analyses were carried out at a stable humidity level, that was guaranteed by an environmental chamber utilised for experimental verification.

First of all, the numerical simulation results were compared with the data given by the experimental test. Thermal strains obtained through the ABAQUS software simulation were in good agreement with the corresponding values given by the FBG sensors utilised in this study. The averaged percentage difference was approximately 5% since the material behaviour changes influenced merely the one temperature.

According to the results given by the experimental tests, the strain values for all sensors embedded in the samples ( $S1_w$ ,  $S2_w$ ,  $S3_w$ ) were the same, and the assumption that the averaged strain of the CFRP specimens were presented was justified. The averaged difference among the strain values determined for the same temperatures is equal to  $4 \times 10^{-6}$ . It was also understood that for the sensors put on the samples surfaces differences were captured which were associated to the FBG sensors location either on the carbon fibre and the matrix ( $S1_z$  and  $S3_z$ ) or on the carbon fibre bundle ( $S2_z$ ).

On the other hand, it was concluded that the strange behaviour of the material above 40 °C was due to the fact that the PLA material inside the CFRP has not a constant CTE value within the temperature elevation range. It was measured experimentally and the CTE value for 20 °C and 40 °C was constant but it was changed above 40 °C. Therefore, the relationship is linear but the parameter is different and depends upon the ranges.

Therefore, the findings of this article could be considered as motivation for further developing AM techniques of composite structures-embedded FBG sensors. Future work will include the effect of different layer orientations of 3D-printed CFRP samples on the accuracy of the results given by the FBG sensors and thermo-mechanical behaviour of structures.

**Author Contributions:** Conceptualisation, T.S. and M.M.; methodology, M.M.; software, T.S. and M.M.; validation, M.M.; formal analysis, M.M.; investigation, T.S. and M.M.; resources, M.M.; writing—original draft preparation, T.S. and M.M.; Writing—Review & Editing, T.S. and M.M.; visualisation, M.M.; supervision, M.M.; project administration, M.M.; funding acquisition, M.M. All authors have read and agreed to the published version of the manuscript.

**Funding:** This research was supported by the project ‘Additive manufactured composite smart structures with embedded fibre Bragg grating sensors (AMCSS)’ funded by the National Science Centre, Poland under M-ERA.NET 2 Call 2019, grant agreement 2019/01/Y/ST8/00075.

**Institutional Review Board Statement:** Not applicable.

**Informed Consent Statement:** Not applicable.

**Data Availability Statement:** Data sharing not applicable.

**Acknowledgments:** The authors of this work would like to thank the researchers from the Kaunas University of Technology, Lithuania for the sample manufacturing. ABAQUS calculations were carried out at the Academic Computer Centre in Gdańsk (Poland).

**Conflicts of Interest:** The authors declare that they have no competing financial interests that could influence the work reported in this study.

#### References

1. Mieloszyk, M.; Andrearczyk, A.; Majewska, K.; Jurek, M.; Ostachowicz, W. Polymeric structure with embedded fiber Bragg grating sensor manufactured using multi-jet printing method. *Measurement* **2020**, *166*, 108229. [[CrossRef](#)]
2. Liu, Z.; Jiang, Q.; Ning, F.; Kim, H.; Cong, W.; Xu, C.; Zhang, H. Investigation of Energy Requirements and Environmental Performance for Additive Manufacturing Processes. *Sustainability* **2018**, *10*, 2018. [[CrossRef](#)]
3. Shafighfard, T.; Cender, T.A.; Demir, E. Additive manufacturing of compliance optimized variable stiffness composites through short fiber alignment along curvilinear paths. *Addit. Manuf.* **2020**, *37*, 101728. [[CrossRef](#)]

4. Cardeal, G.; Sequeira, D.; Mendonça, J.; Leite, M.; Ribeiro, I. Additive manufacturing in the process industry: A process-based cost model to study life cycle cost and the viability of additive manufacturing spare parts. *Procedia CIRP* **2021**, *98*, 211–216. [[CrossRef](#)]
5. Shafighfard, T.; Demir, E.; Yildiz, M. Design of fiber-reinforced variable-stiffness composites for different open-hole geometries with fiber continuity and curvature constraints. *Compos. Struct.* **2019**, *226*, 111280. [[CrossRef](#)]
6. Munghen, D.; Iacobellis, V.; Behdinan, K. Incorporation of fiber Bragg grating sensors in additive manufactured Acrylonitrile butadiene styrene for strain monitoring during fatigue loading. *Int. J. Fatigue* **2022**, *154*, 106485. [[CrossRef](#)]
7. Minakuchi, S.; Takeda, N.; Takeda, S.I.; Nagao, Y.; Franceschetti, A.; Liu, X. Life cycle monitoring of large-scale CFRP VARTM structure by fiber-optic-based distributed sensing. *Compos. Part A Appl. Sci. Manuf.* **2011**, *42*, 669–676. [[CrossRef](#)]
8. Kinet, D.; Mégret, P.; Goossen, K.W.; Qiu, L.; Heider, D.; Caucheteur, C. Fiber Bragg grating sensors toward structural health monitoring in composite materials: Challenges and solutions. *Sensors* **2014**, *14*, 7394–7419. [[CrossRef](#)]
9. Matveenko, V.; Kosheleva, N.; Serovaev, G.; Fedorov, A. Analysis of Reliability of Strain Measurements Made with the Fiber Bragg Grating Sensor Rosettes Embedded in a Polymer Composite Material. *Sensors* **2021**, *21*, 5050. [[CrossRef](#)]
10. Mieloszyk, M.; Majewska, K.; Ostachowicz, W. Application of embedded fibre Bragg grating sensors for structural health monitoring of complex composite structures for marine applications. *Mar. Struct.* **2021**, *76*, 102903. [[CrossRef](#)]
11. Basu, M.; Ghorai, S. Sequential interrogation of multiple FBG sensors using LPG modulation and an artificial neural network. *Meas. Sci. Technol.* **2015**, *26*, 045104. [[CrossRef](#)]
12. Leng, J.; Asundi, A. Structural health monitoring of smart composite materials by using EFPI and FBG sensors. *Sens. Actuators A Phys.* **2003**, *103*, 330–340. [[CrossRef](#)]
13. Quan, Z.; Wu, A.; Keefe, M.; Qin, X.; Yu, J.; Suhr, J.; Byun, J.H.; Kim, B.S.; Chou, T.W. Additive manufacturing of multi-directional preforms for composites: Opportunities and challenges. *Mater. Today* **2015**, *18*, 503–512. [[CrossRef](#)]
14. Mieloszyk, M. Fatigue Crack Propagation Monitoring Using Fibre Bragg Grating Sensors. *Vibration* **2021**, *4*, 700–721. [[CrossRef](#)]
15. Chen, J.; Wang, J.; Li, X.; Sun, L.; Li, S.; Ding, A. Monitoring of temperature and cure-induced strain gradient in laminated composite plate with FBG sensors. *Compos. Struct.* **2020**, *242*, 112168. [[CrossRef](#)]
16. Arena, M.; Viscardi, M. Strain state detection in composite structures: Review and new challenges. *J. Compos. Sci.* **2020**, *4*, 60. [[CrossRef](#)]
17. Lau, K. Structural health monitoring for smart composites using embedded FBG sensor technology. *Mater. Sci. Technol.* **2014**, *30*, 1642–1654. [[CrossRef](#)]
18. Oromiehie, E.; Prusty, B.G.; Compston, P.; Rajan, G. Characterization of process-induced defects in automated fiber placement manufacturing of composites using fiber Bragg grating sensors. *Struct. Health Monit.* **2018**, *17*, 108–117. [[CrossRef](#)]
19. Homa, D.; Hill, C.; Floyd, A.; Pickrell, G.; Hall, H. Fiber Bragg gratings embedded in 3D printed prototypes. *Sci. Adv. Today* **2016**, *2*, 25242.
20. Mieloszyk, M.; Majewska, K.; Andrearczyk, A. Influence of Temperature on Additive Manufacturing Polymer Structure with Embedded Fibre Bragg Grating Sensors. In *European Workshop on Structural Health Monitoring*; Springer: Berlin/Heidelberg, Germany, 2020; pp. 679–686.
21. Kousiatza, C.; Karalekas, D. In-situ monitoring of strain and temperature distributions during fused deposition modeling process. *Mater. Des.* **2016**, *97*, 400–406. [[CrossRef](#)]
22. Economidou, S.N.; Karalekas, D. Optical sensor-based measurements of thermal expansion coefficient in additive manufacturing. *Polym. Test.* **2016**, *51*, 117–121. [[CrossRef](#)]
23. Zhong, W.; Li, F.; Zhang, Z.; Song, L.; Li, Z. Short fiber reinforced composites for fused deposition modeling. *Mater. Sci. Eng. A* **2001**, *301*, 125–130. [[CrossRef](#)]
24. Ning, F.; Cong, W.; Qiu, J.; Wei, J.; Wang, S. Additive manufacturing of carbon fiber reinforced thermoplastic composites using fused deposition modeling. *Compos. Part B Eng.* **2015**, *80*, 369–378. [[CrossRef](#)]
25. Ibrahim, Y.; Melenka, G.W.; Kempers, R. Fabrication and tensile testing of 3D printed continuous wire polymer composites. *Rapid Prototyp. J.* **2018**, *24*, 1131–1141. [[CrossRef](#)]
26. Dugbenoo, E.; Arif, M.F.; Wardle, B.L.; Kumar, S. Enhanced Bonding via Additive Manufacturing-Enabled Surface Tailoring of 3D Printed Continuous-Fiber Composites. *Adv. Eng. Mater.* **2018**, *20*, 1800691. [[CrossRef](#)]
27. Chacón, J.; Caminero, M.; Núñez, P.; García-Plaza, E.; García-Moreno, I.; Reverte, J. Additive manufacturing of continuous fibre reinforced thermoplastic composites using fused deposition modelling: Effect of process parameters on mechanical properties. *Compos. Sci. Technol.* **2019**, *181*, 107688. [[CrossRef](#)]
28. Kabir, S.F.; Mathur, K.; Seyam, A.F.M. A critical review on 3D printed continuous fiber-reinforced composites: History, mechanism, materials and properties. *Compos. Struct.* **2020**, *232*, 111476. [[CrossRef](#)]
29. Syrlybayev, D.; Zharylkassyn, B.; Seisekulova, A.; Akhmetov, M.; Perveen, A.; Talamona, D. Optimisation of Strength Properties of FDM Printed Parts—A Critical Review. *Polymers* **2021**, *13*, 1587. [[CrossRef](#)]
30. Wickramasinghe, S.; Do, T.; Tran, P. FDM-based 3D printing of polymer and associated composite: A review on mechanical properties, defects and treatments. *Polymers* **2020**, *12*, 1529. [[CrossRef](#)] [[PubMed](#)]
31. Li, Y.; Feng, Z.; Hao, L.; Huang, L.; Xin, C.; Wang, Y.; Bilotti, E.; Essa, K.; Zhang, H.; Li, Z.; et al. A review on functionally graded materials and structures via additive manufacturing: from multi-scale design to versatile functional properties. *Adv. Mater. Technol.* **2020**, *5*, 1900981. [[CrossRef](#)]

32. Guessasma, S.; Belhabib, S.; Nouri, H. Effect of printing temperature on microstructure, thermal behavior and tensile properties of 3D printed nylon using fused deposition modeling. *J. Appl. Polym. Sci.* **2021**, *138*, 50162. [[CrossRef](#)]
33. Paul, S. Finite Element Analysis in Fused Deposition Modeling Research: A Literature Review. *Measurement* **2021**, *178*, 109320. [[CrossRef](#)]
34. Economidou, S.N.; Karalekas, D. Characterization of fused deposition modeling polymeric structures using embedded fiber Bragg grating sensors. In *Additive Manufacturing*; Elsevier: Amsterdam, The Netherlands, 2018; pp. 163–180.
35. Kantaros, A.; Karalekas, D. FBG based in situ characterization of residual strains in FDM process. In *Residual Stress, Thermo-mechanics & Infrared Imaging, Hybrid Techniques and Inverse Problems*; Springer: Berlin/Heidelberg, Germany, 2014; Volume 8, pp. 333–337.
36. Kousiatza, C.; Tzetzis, D.; Karalekas, D. In-situ characterization of 3D printed continuous fiber reinforced composites: A methodological study using fiber Bragg grating sensors. *Compos. Sci. Technol.* **2019**, *174*, 134–141. [[CrossRef](#)]
37. Mekid, S.; Daraghma, H. Manufacturing Processes of Sensorial Materials: Sensors Placement and Experimental Validation. *Iop Conf. Ser. Mater. Sci. Eng.* **2019**, *538*, 012014. [[CrossRef](#)]
38. Hong, C.; Bao, C.; Fei, J.; Zhang, Y.; Wang, X. Application of FBG Technology in Additive Manufacturing: Monitoring Real-time Internal Temperature of Products. *IEEE Sens. J.* **2020**, *21*, 6003–6011. [[CrossRef](#)]
39. Kousiatza, C.; Karalekas, D. Experimental study of fabrication-induced residual strains and distortions in polymeric square plates built using fused deposition modeling process. *Mater. Des. Process. Commun.* **2021**, *3*, e149. [[CrossRef](#)]
40. Muna, I.I.; Mieloszyk, M. Temperature Influence on Additive Manufactured Carbon Fiber Reinforced Polymer Composites. *Materials* **2021**, *14*, 6413. [[CrossRef](#)] [[PubMed](#)]
41. Rimašauskas, M.; Kuncius, T.; Rimašauskienė, R. Processing of carbon fiber for 3D printed continuous composite structures. *Mater. Manuf. Process.* **2019**, *34*, 1528–1536. [[CrossRef](#)]
42. Cristea, M.; Ionita, D.; Iftime, M.M. Dynamic mechanical analysis investigations of pla-based renewable materials: How are they useful? *Materials* **2020**, *13*, 5302. [[CrossRef](#)]
43. *ABAQUS/Standard User's Manual*; Version 6.14; Dassault Systèmes Simulia Corp: Providence, RI, USA, 2017.